OXFORD

ORIGINAL ARTICLE

Altered Dynein Axonemal Assembly Factor 1 Expression in C-Boutons in Bulbar and Spinal Cord Motor-Neurons in Sporadic Amyotrophic Lateral Sclerosis

Pol Andrés-Benito, Mr, Mònica Povedano, MD, Pascual Torres, Mr, Manuel Portero-Otín, PhD, and Isidro Ferrer, MD, PhD

Abstract

Dyneins are major components of microtubules. Dynein assembly is modulated by a heterogeneous group of dynein axonemal assembly factors (DNAAFs). The present study analyzes dynein axonemal assembly factor 1 (*DNAAF1*) and leucine-rich repeat-containing protein 50 (LRRC50), the corresponding encoded protein, in lower motor neurons in spinal cord of sALS postmortem samples and *hSOD1-G93A* transgenic mice compared with controls. *DNAAF1* mRNA is significantly reduced in the anterior horn in sALS, and LRRC50 immunoreactivity is significantly reduced in C-boutons of the remaining motor neurons of the anterior horn, dorsal nucleus of the vagus nerve, and hypoglossal nuclei at terminal stages of ALS. LRRC50 immunoreactivity has a perinuclear distribution in motor neurons in sALS thus suggesting a disorder of transport. The number of LRRC50-/S1R-immunoreactive structures is also significantly decreased in *hSOD1-G93A* transgenic mice at the age of 90 days (preclinical stages), and the number of motor neurons with LRRC50-immunoreactive structures is significantly reduced in animals aged 150 days (clinical stages). These observations suggest cholinergic denervation of motor neurons as a pathogenic factor in motor neuron disease. LRRC50 protein levels were not detected in human CSF.

Key Words: Amyotrophic lateral sclerosis, Biomarkers, Dynein axonemal assembly factor 1, LRRC50, Motor-neurons, Spinal cord.

INTRODUCTION

Neuronal microtubules are intracellular structures that facilitate a myriad of neuronal functions, including activity-dependent axonal transport (1), which is governed by the dynein/kinesin system (2, 3). Anterograde transport, mediated by kinesins, supplies distal axons with newly synthesized proteins and lipids, including synaptic components required to maintain presynaptic activity, whereas retrograde transport, mediated by dyneins, is required to maintain homeostasis by removing aging proteins and organelles from the distal axon for degradation and recycling of components (1, 3).

Dynein is a dimer composed of the motor-containing heavy chain and the distal tail formed by intermediate chains, light intermediate chains, and light chains. The motor domain is in the C-terminus and is responsible for microtubule binding, inasmuch as the N-terminal tail domain is responsible for dimerization, dynein interaction with other proteins (e.g. dynactin), and cargo interaction (3–6).

Amyotrophic lateral sclerosis (ALS) is a multifactorial disease characterized by the degeneration of motor neurons, their axons, and neuromuscular synapses (7, 8). Microtubule alterations, including abnormal kinesin/dynein and related interactors, are critical factors in the pathogenesis of this disease (9–18). In addition, Golgi complex disruption results from abnormal dynein/dynactin interactions (6). Since recent transcriptomics observations have identified significant reduction in the expression of a cluster involving several axonemal dynein transport components in the anterior horn of the spinal cord (SC) in sporadic ALS (sALS) (19), the ensuing study analyzes dynein axonemal assembly factor 1 (*DNAAF1*) and leucine-rich repeat-containing protein 50 (LRRC50), the corresponding encoded protein, in lower motor neurons in sALS compared with controls. LRRC50 is a dynein up-stream effector that participates in the cytoplasmic preassembly of dynein arms and is involved in the regulation of microtubule-based cilia and actin-based brush border microvilli. Different mutations in LRRC50 result in distinct clinical syndromes,

including abnormal assembly of cilia in respiratory epithelia producing primary ciliary dyskinesia, altered cardiac laterality, and polycystic kidney (20–22). The distribution and localization of LRRC50 in the nervous system is not known. The present study has identified LRRC50 in C-boutons of motor neurons of the SC and selected motor nuclei of the brain stem in sALS, and decreased LRRC50 immunoreactivity in sALS and in SOD1 transgenic mice as a model of unrelated motor neuron disease.

MATERIALS AND METHODS

Human Tissue Samples

Paraffin-embedded postmortem fresh-frozen and 4% formalin-fixed samples of the lumbar SC and medulla oblongata were obtained from the Institute of Neuropathology HUB-ICO-IDIBELL Biobank following the guidelines of the Spanish legislation (Real Decreto de Biobancos 1716/2011) and the approval of the local ethics committee of the Bellvitge University Hospital-Institute of Biomedical Research IDI-BELL. The postmortem interval between death and tissue processing was from 2 to 17 hours. Transversal sections of the SC were alternatively frozen at –80°C or fixed by immersion in 4% buffered formalin. Age-matched control cases had not suffered from neurologic or psychiatric diseases and did not have neuropathologic lesions. Genetic testing, using genomic DNA isolated from blood or brain tissue, revealed no mutations in the chromosome 9 open reading frame (*C9orf72*), superoxide dismutase 1 (*SOD1*), TAR DNA binding protein (*TARDBP*), or FUS RNA binding protein (*FUS*). Cases in the present series used for biochemical studies (i.e. quantitative reverse transcription PCR [RT-qPCR]) are summarized in the Table. Cases used for immunohistochemical studies did not correspond always with those of the biochemical series; this group was composed of 16 sALS 10 age-matched controls as described in the corresponding section. Variable numbers of TDP-43-P-immunoreactive neuronal and oligodendroglial inclusions and neuropil threads were found in the anterior horn of the SC in every ALS case. Neuronal inclusions were small, round intracytoplasmic deposits, large globular inclusions and skein-like inclusions. Neuronal inclusions were present in only ∼20% of the remaining motor neurons in ALS.

Animal Model hSOD1-G93A

Transgenic mice expressing high copy numbers of the mutated form of human SOD1 (hSOD1), B6SJL-Tg(SOD1*G93A)1Gur/J (*hSOD1-G93A*) were obtained from The Jackson Laboratories (Bar Harbor, ME). The colony was maintained by breeding male hemizygous carriers with nontransgenic B6SJL females. Offspring were identified by PCR, and non-transgenic G93A littermates were used as wild-type controls. In addition, unrelated WT mice were examined. Animals were maintained under standard animal housing conditions (static isolation caging, 3–4 animals per cage) in a 12-hour dark-light cycle with free access to food and water. The first series of immunohistochemical studies was performed on 5 *hSOD1-G93A* mice, 3 control littermates, and 3 WT aged 150 days. The second series of histochemical studies

TABLE. Summary of Cases Used for Biochemical Study

Case	Age	Gender	Diagnosis	PM Delay	Initial Symptoms	RIN Value SC
1	59	M	Control	12 h 05 min	–	6.4
2	43	M	Control	05 h 55 min	–	6.6
3	47	M	Control	04 h 55 min	–	5.6
4	64	F	Control	11 h 20 min	–	6.2
5	46	M	Control	15 h 00 min	–	5.9
6	56	M	Control	07 h 10 min	–	6.1
7	71	F	Control	08 h 30 min	–	5.9
8	64	F	Control	05 h 00 min	–	7.0
9	79	F	Control	06 h 25 min	–	6.7
10	75	M	Control	07 h 30 min	–	5.0
11	55	M	Control	09 h 45 min	–	5.3
12	76	M	Control	06 h 30 min	–	6.6
13	51	F	Control	04 h 00 min	–	6.3
14	56	M	sALS	10 h 50 min	N/A	7.1
15	70	M	sALS	03 h 00 min	Respiratory	7.3
16	77	M	sALS	04 h 30 min	N/A	7.4
17	56	F	sALS	03 h 45 min	N/A	8.2
18	59	M	sALS	03 h 15 min	N/A	7.5
19	63	F	sALS	13 h 50 min	Bulbar	6.8
20	59	F	sALS	14 h 15 min	N/A	6.4
21	64	M	sALS	16 h 30 min	N/A	6.3
22	57	F	sALS	04 h 00 min	Bulbar	6.2
23	75	F	sALS	04 h 05 min	Bulbar	6.8
24	79	F	sALS	02 h 10 min	N/A	7.0
25	57	F	sALS	10 h 00 min	Bulbar	6.5
26	46	M	sALS	07 h 00 min	Spinal	7.0
27	69	F	sALS	17 h 00 min	Spinal	6.4

Abbreviations: sALS, sporadic amyotrophic lateral sclerosis cases; M, male; F, female; PM delay, postmortem delay (hours, minutes); N/A, not available; RIN, RNA integrity number.

was carried out on the SCs of 5 animals per stage: 90 days (preclinical), 120 (early clinical), and 150 (late clinical). Genotyped mice were dissected for immunohistochemical studies. All the procedures were carried out after the approval of the Animal Ethics Committee of the University of LLeida.

RNA Extraction and RT-qPCR

RNA from dissected human frozen anterior horn of the lumbar SC of 14 sALS (mean age 61 years; 6 men and 8 women) and 13 age-matched controls (mean age 59 years; 8 men and 5 women) was extracted following the instructions of the supplier (RNeasy Mini Kit, Qiagen, Hilden, Germany). RNA integrity and 28S/18S ratios were determined with the Agilent Bioanalyzer (Agilent Technologies, Santa Clara, CA) to assess RNA quality, and the RNA concentration was evaluated using a NanoDrop Spectrophotometer (Thermo Fisher Scientific, Waltham, MA). Complementary DNA (cDNA) preparation used the High-Capacity cDNA Reverse Transcription kit (Applied Biosystems, Foster City, CA) following the protocol provided by the supplier. Parallel reactions for each RNA sample were run in the absence of MultiScribe Reverse

Transcriptase to assess the lack of contamination of genomic DNA. TaqMan RT-qPCR assays for *DNAAF1* (Hs00698 399_m1) were performed as detailed elsewhere (19). Hypoxanthine-guanine phosphoribosyltransferase (*HPRT1*) was used as internal control for normalization of SC samples. The double-delta cycle threshold ($\Delta\Delta CT$) method was utilized to determine the fold change values. The obtained data were analyzed with the *t*-test.

Immunohistochemistry

Dewaxed 4-µm-thick sections of the SC and medulla oblongata in human cases and SC in mice were processed for immunohistochemistry. The human series included 16 sALS (mean age 57 years; 6 men and 8 women) and 10 age-matched controls (mean age 62 years; 6 men and 4 women). Immunohistochemistry in murine SCs was performed in 5×3 transgenic mice (5 animals at the ages of 90, 120, and 150 days) and 3×2 controls (3 control littermates and 3 WT aged 150 days). The sections were boiled in citrate buffer (20 minutes) to retrieve protein antigenicity. Endogenous peroxidases were blocked by incubation in 10% methanol-1% H_2O_2 solution (15 minutes) followed by 3% normal horse serum solution. Then the sections were incubated at 4°C overnight with one of the primary antibodies: LRRC50 (1/200, polyclonal rabbit, Abcam, Cambridge, UK); vesicular acetylcholine transporter: VAChT (1/100, polyclonal guinea pig, Synaptic Systems, Goettingen, Germany); and sigma 1 receptor: S1R (1/100, monoclonal mouse, Santa Cruz Biotechnology, Santa Cruz, CA). Following incubation with the primary antibody, the sections were incubated with EnVision + system peroxidase (Dako, Agilent Technologies) for 30 minutes at room temperature. The peroxidase reaction was visualized with diaminobenzidine and H_2O_2. Control of the immunostaining included omission of the primary antibody; no signal was obtained following incubation with only the secondary antibodies. No positive controls were used.

Double-Labeling Immunofluorescence and Confocal Microscopy

Dewaxed 4-µm-thick sections of human and mouse control SCs were stained with a saturated solution of Sudan black B (Merck, Glostrup, Denmark) for 15 minutes to block the autofluorescence of lipofuscin granules present in cell bodies, and then rinsed in 70% ethanol and washed in distilled water. The sections of human cases were incubated at 4°C overnight with double combinations (double-labeling) of LRRC50 (1/200, polyclonal rabbit, Abcam, Cambridge, UK) and VAChT (1/100, polyclonal guinea pig, Synaptic Systems) or S1R (1/100, monoclonal mouse, Santa Cruz Biotechnology) or synaptophysin (monoclonal mouse antibody used at 1/500, Leica Biosystems, Wetzlar, Germany) or TDP43-P Ser409/ Se410 (1:200, MABN14 rat, Millipore, Burlington, MA). Other sections were triple labeled with LRRC50, VAChT, and S1R. The sections of mice were processed for double-labeling immunofluorescence with antiLRRC50 and antiS1R antibodies. After washing, the sections were incubated with the respective fluorescence secondary antibodies Alexa555, Alexa488,

and/or Alexa657 (1:400, Molecular Probes, Eugene, OR) against the corresponding host species. Nuclei were stained with DRAQ5 (dilution 1:2000, BioStatus, Loughborough, UK). After washing, the sections were mounted in Immuno-Fluore mounting medium (ICN Biomedicals, Irvine, CA), sealed, and dried overnight. Sections were examined with a Leica TCS-SL confocal microscope. Control of the immunostaining included omission of the primary antibody; no signal was obtained following incubation with only the secondary antibodies.

Quantification and Statistical Analysis

Quantification of LRRC50 expression in human histological sections was made directly from the ocular of the microscope at a magnification of $\times 200$ by counting the number of motor-neurons containing LRRC50-positive boutons in (i) the whole anterior horn of the lumbar SC, (ii) motor nucleus of the vagus nerve, and (iii) hypoglossal nucleus (HN) in 3 different sections separated 100 µm for every region in every sALS and control case. A similar approach was used to quantify motor-neurons with VAChT- and S1R-positive structures. Quantitative studies in mice were carried out only in the ventral horn of the SC following the same protocol. Quantification was made by one person blinded to the clinical status. The normality of distribution of counted cell number was analyzed with the Kolmogorov-Smirnov test. The unpaired *t*-test was performed to compare each group when values followed a normal distribution. Statistical analysis and graphic design were performed with GraphPad Prism version 5.01 (La Jolla, CA). Results were analyzed with the Student *t*-test. Outliers were detected using the GraphPad software QuickCalcs (p < 0.05). The data were expressed as mean ± SEM and significance levels were set at *p < 0.05, **p < 0.01, and ***p < 0.001.

ELISA in CSF

Samples were obtained from sALS patients and controls as detailed elsewhere (23). CSF (1.5 ± 0.5 mL) was collected in polypropylene tubes as part of the clinical routine investigation. CSF was centrifuged at 3000 rpm for 15 minutes at room temperature. Supernatant was collected and aliquoted in volumes of 250 µL and stored at –80°C until use. All samples were analyzed after one freeze/thaw cycle. Quantification of LRRC50 was performed using the Human Dynein assembly factor 1, axonemal, LRRC50 ELISA Kit (Catalogue N° MBS9317767, MyBiosource, San Diego, CA) following the manufacturer's instructions.

RESULTS

In agreement with a previous study (19), *DNAAF1* mRNA expression levels in the anterior horn of the SC were significantly reduced in sALS compared with controls (p = 0.019; Fig. 1A).

LRRC-50 immunoreactivity in the human control SC and brainstem was restricted to immunoreactive boutons in motor neurons, and walls in the blood vessels. Such boutons were elongated, oval-shaped, 1–5 µm in length, and mainly localized at the periphery of the cytoplasm near the plasma

3
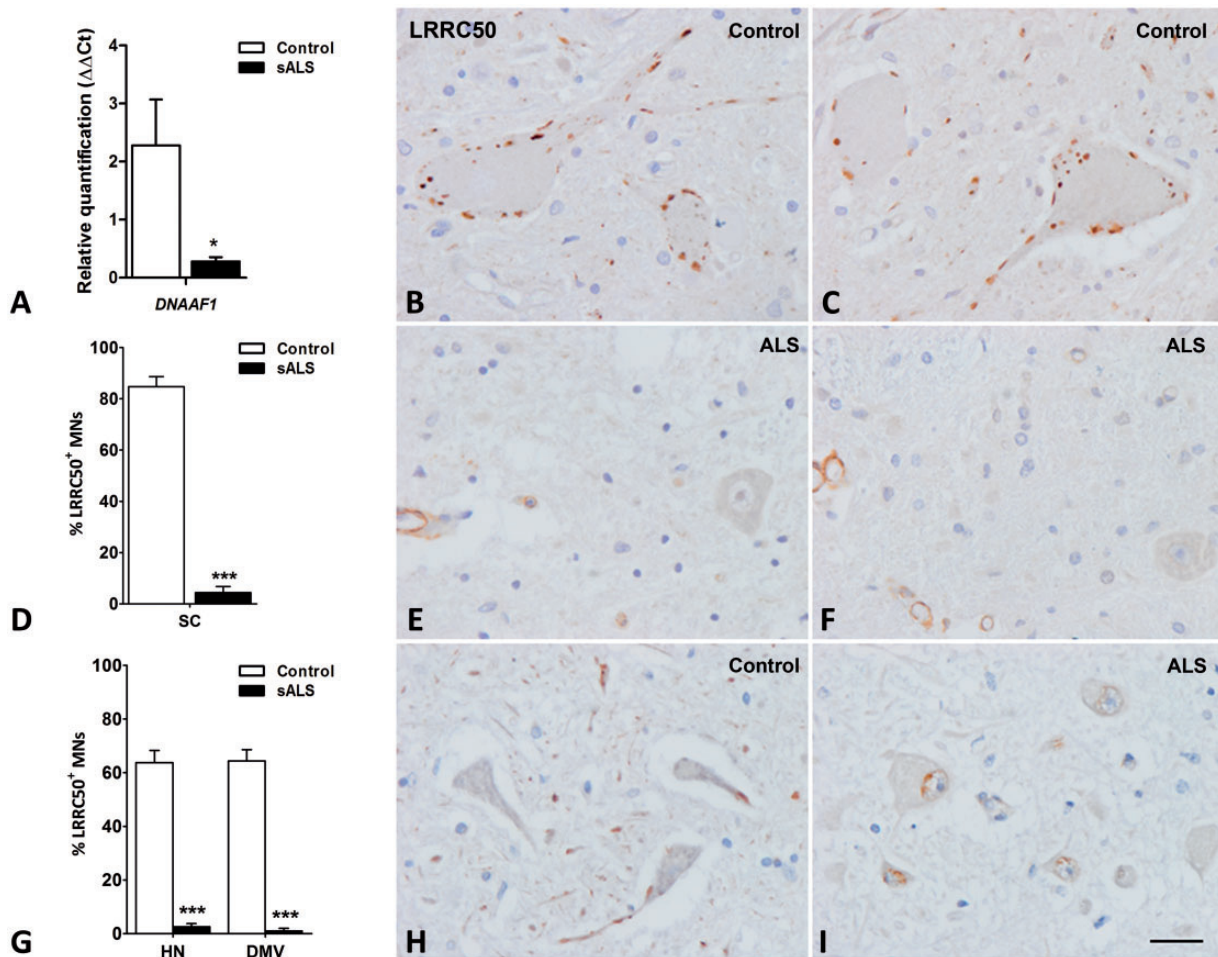
FIGURE 1. *DNAAF1* and LRRC50 expression in human control and sALS lower motor neurons. **(A)** Reduced *DNAAF1* mRNA expression in the anterior horn of the lumbar spinal cord in sALS compared with age-matched controls. **(B, C)** LRRC50 immunoreactivity in anterior horn motor neurons in controls identifies oval-shaped structures (boutons) at the periphery of the cytoplasm and proximal dendrites. **(D)** The percentage of motor neurons with LRRC50-immunoreactive dots is significantly decreased in the anterior horn of the spinal cord (SC) in sALS when compared with controls. **(E, F)** This decrease is due to the almost total absence of LRRC50-positive boutons in the remaining sALS motor neurons. **(G)** Similar reduction is found in the hypoglossal nucleus (HN) and motor nucleus of the vagus nerve (DNV) in sALS when compared with controls. **(H, I)** Representative images of the motor nucleus of the vagus nerve in control and sALS showing marked reduction, almost absence of LRRC50-immunoreactive boutons. Note perinuclear LRRC50 immunoreactivity in some motor neurons in sALS (arrows) but not in controls. LRRC50 immunoreactivity is also present in capillaries (ca). Paraffin sections slightly counterstained with hematoxylin; scale bar = 25 μm. Unpaired *t*-test, *p < 0.05, ***p < 0.001.

membrane of the cell body and proximal dendrites (Fig. 1B, C). The number of LRRC50-immunoreactive boutons per neuron was as high as twenty-five in a single paraffin section. However, the number of LRRC50-immunoreactive boutons was markedly reduced in the remaining motor neurons in the anterior horn of the SC in sALS cases (p = 1.10×10^{-18}; Fig. 1D–F). Similar LRRC50-immunoreactive boutons were found in contact with the cytoplasm and proximal dendrites of motor neurons in the dorsal motor nucleus of the vagus nerve and the HN in control cases, but their number was smaller in comparison with anterior horn motor neurons. A similar reduction in the number of LRRC50-immunoreactive boutons was found in the remaining motor neurons in the dorsal motor nucleus of the vagus nerve (p = 1.2×10^{-7}) and in the HN

(p = 4.3×10^{-8}) in sALS (Fig. 1G–I). Curiously, LRRC50 in several motor neurons in sALS had a perinuclear distribution instead of its presence in boutons (Fig. 1I).

In contrast to the motor nuclei of the hypoglossal nuclei and vagus nerves, LRRC50-positive boutons were absent in the oculomotor nuclei of the brainstem in normal (control) brains (data not shown).

LRRC50 structures were similar in morphology to C-boutons on motor neurons of the spinal horn, as revealed by vesicular acetylcholine transporter (VAChT) and sigma 1 receptor (S1R) immunohistochemistry (Fig. 2). Moreover, VAChT- and S1R-positive motor neuron boutons were largely decreased in sALS cases (p = 8.75×10^{-6} and p = 1.15×10^{-12}, respectively; Fig. 2E, H).
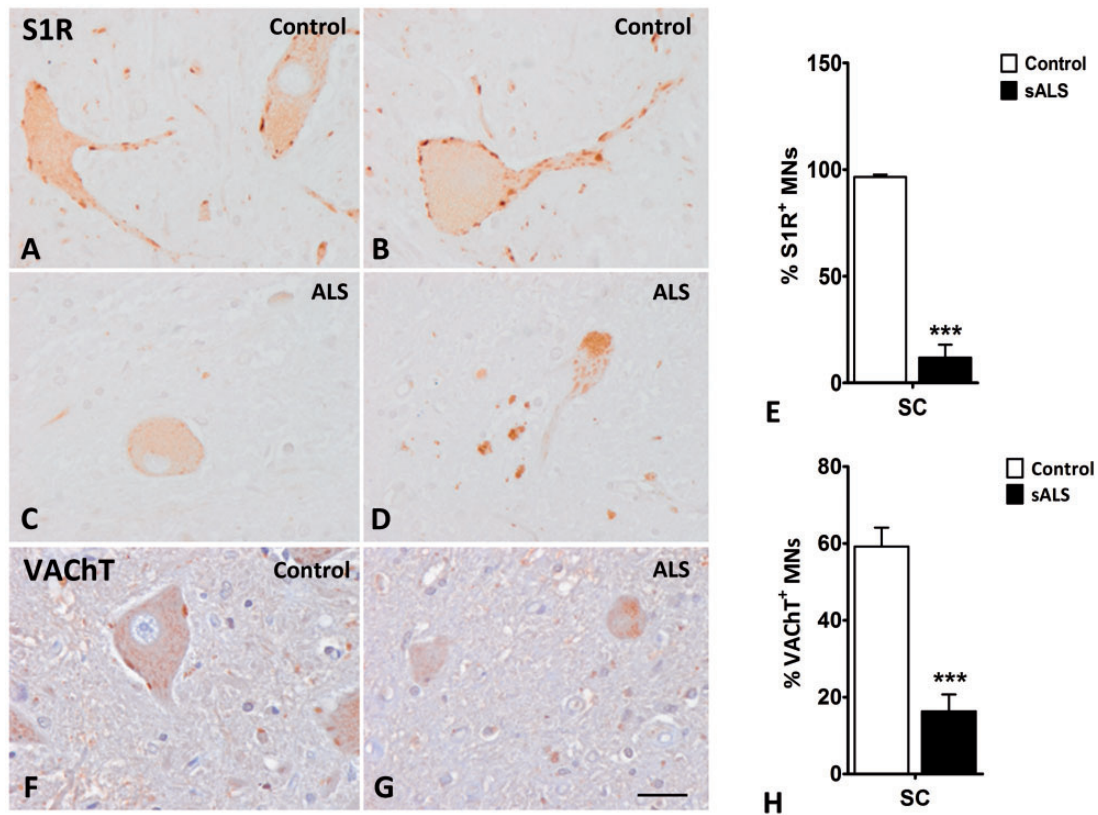
FIGURE 2. Sigma 1 receptor (S1R) and vesicular acetylcholine transporter (VAChT) immunoreactivity in motor neurons of the spinal cord in control and sALS. **(A, B)** S1R-immunoreactive C-boutons are found at the surface of the cytoplasm and proximal dendrites in controls. **(C, D)** Immunoreactive C-boutons practically disappear in the remaining motor neurons in sALS. **(E)** The graph illustrates that the percentage of neurons with S1R-positive C-boutons is significantly decreased in sALS compared with controls. **(F, G)** Representative images of VAChT-immunoreactive C-boutons in control and ALS; remaining ALS motor neurons are almost devoid of VAChT C-boutons. **(H)** The graph illustrates the significant reduction of the percentage of neurons with VAChT-positive C-boutons in sALS compared with controls. Paraffin sections slightly counterstained with hematoxylin; scale bar = 25 μm. Unpaired *t*-test, ***p < 0.001.
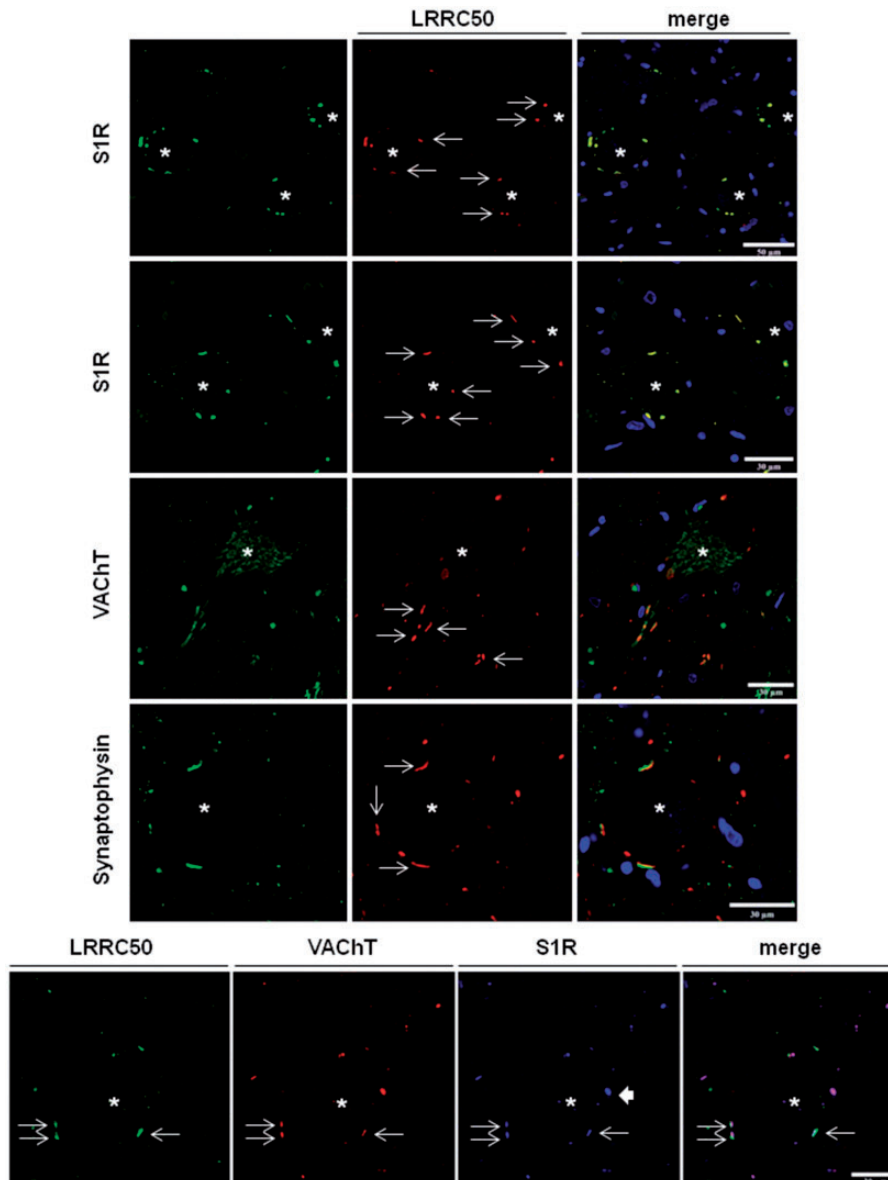
Double- and triple-labeling immunofluorescence to LRRC50 and S1R, VAChT, and synaptophysin in controls showed that LRRC50-immunoreactive boutons colocalized or were in close contact with VAChT or with S1R and synaptophysin-immunoreactive C-boutons (Fig. 3), thus supporting the idea that LRRC50 was a component of C-boutons. Double-labeling immunofluorescence and confocal microscopy to LRRC50 and TDP-43-P showed that loss of C-boutons was found equally in neurons with and without TDP-43-P-immunoreactive inclusions. This was not unexpected as TDP-43-P inclusions were observed in a minority of remaining motor neurons in ALS whereas loss of LRRC50 boutons was generalized in the anterior horn of the SC in ALS (data not shown).

Motor neurons of the SC in control mice (SOD1 littermates and WT mice) showed similar oval or round LRRC50-immunoreactive structures in the cytoplasm (Fig. 4). LRRC50-positive structures were in close proximity or colocalized with S1R as revealed by double-labeling immunofluorescence and confocal microscopy (Fig. 4). No differences were seen between control littermates and WT mice at the age of 150 days. However, LRRC50 positivity was significantly decreased in motor neurons in *hSOD1-G93A* transgenic mice aged 150 days (p = 0.001; Fig. 4).

To learn whether loss of LRRC50 immunoreactivity was an early or a late event in the progression of motor neuron degeneration, *hSOD1-G93A* transgenic mice at preclinical and early clinical stages, 90 and 120 days old, respectively, were examined. As shown in Figure 5, the number of positive structures per neuron was already decreased at the age of 90 days (preclinical stage) in hSOD1-G93A transgenic mice compared with controls (p = 0.03). The reduction was still noted at the age of 120 days although it was not significant (p = 0.14).

Finally, to test whether LRRC50 in the CSF might serve as a complementary biomarker in sALS, LRRC50 levels were measured using a commercial quantitative sandwich ELISA kit. The detection range was from 3.12 ng/mL to 100 ng/mL. Levels of LRRC50 were not detectable in the CSF of controls and sALS cases.

5

FIGURE 3. Double-labeling (upper panel) and triple-labeling (lower panel) immunofluorescence and confocal microscopy to LRRC50 and sigma 1 receptor (S1R), vesicular acetylcholine transporter (VAChT) or synaptophysin (SYN) in normal motor neurons of the human lumbar spinal cord. Upper panel: LRRC50-immunoreactive boutons (red) colocalize S1R-immunoreactive C-boutons (green), VAChT-positive C-boutons (green), and large synaptophysin terminals (green) at the periphery of the cytoplasm and proximal dendrites (arrows) of motor neurons (asterisks). Merge shows, in addition, nuclei stained with DRAQ5 (blue). Lower panel: LRRC50 (green) colocalizes VAChT (red) and S1R (blue) in C-boutons (long arrows: merge: white); some structures colocalize VAChT and S1R but not VAChT (thick arrow). Paraffin sections; scale bar = 30 μm except upper row in which bar = 50 μm.

DISCUSSION

Dynein processing and localization varies in different cell types and clusters in distinct subcellular organelles (24–27). In the central nervous system, dyneins are largely localized at the axon terminals (27). Dynein assembly is modulated by a heterogeneous group of DNAAFs that act, in most instances, in combination with particular chaperones to promote cytoplasmic pre-assembly of dyneins (28–33).

Mutations in certain DNAAFs such as *NADYX1C1*, *ZYYND10*, *C11orf70* (encoding CFAP300: cilia and flagella associated protein 300), and *PIH1D3* result in abnormal dynein assembly (30, 34–40). Likewise, mutations in *DNAAF1* result in abnormal assembly of cilia in respiratory epithelia, infertility, altered cardiac laterality, and polycystic kidney (20–22).

The present study identifies the presence of LRRC50-immunoreactive boutons at the surface of motor neurons of the
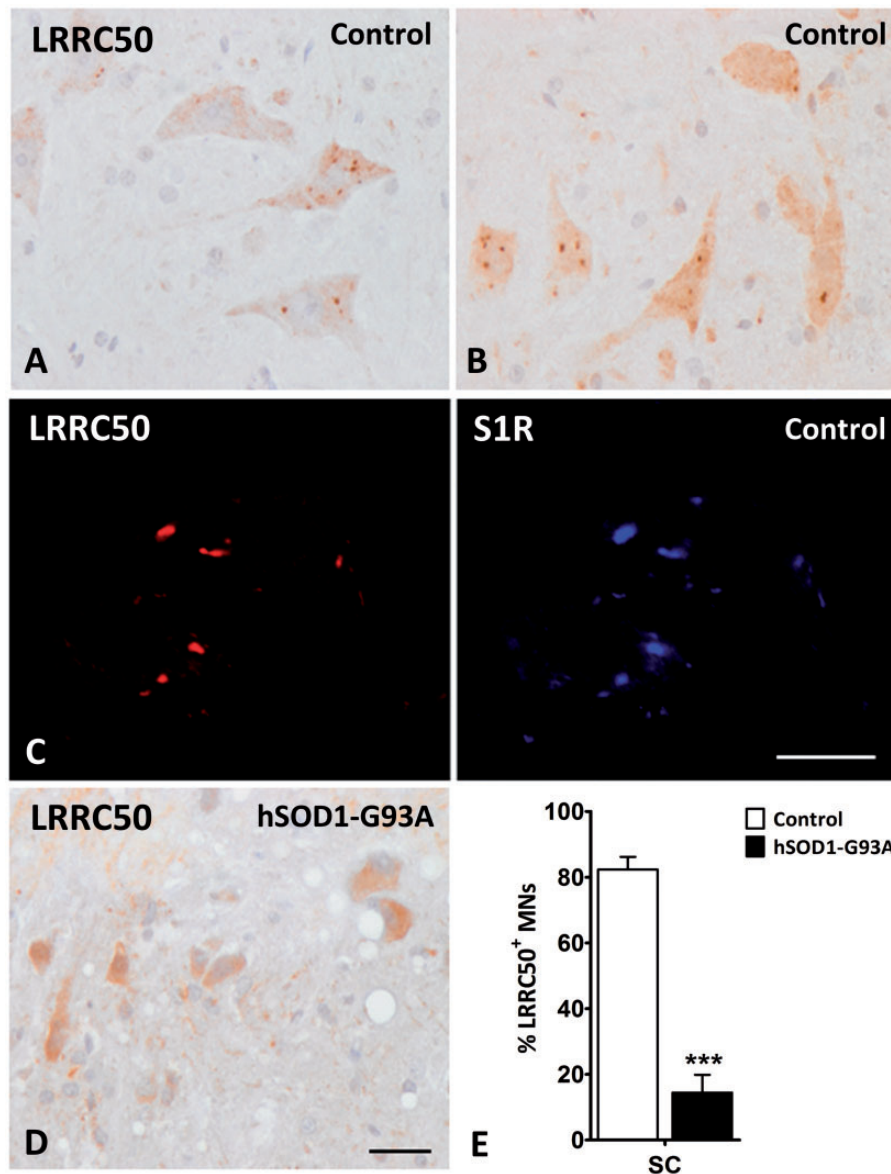
FIGURE 4. LRRC50-immunoreactive boutons in motor neurons of the spinal cord in mice. **(A, B)** LRRC-50 immunoreactivity is found in cytoplasmic structures in control mice. **(C)** Double-labeling immunofluorescence and confocal microscopy depicts close proximity and partial colocalization of LRRC50 (green) and S1R (red) immunoreactivity. **(D)** LRRC50 immunoreactivity is almost depleted in motor neurons in *hSOD1-G93A* transgenic mice aged 150 days (clinical stage). **(E)** Quantification of motor-neurons with LRRC50-positive structures is significantly reduced in transgenic mice when compared with wild type littermates. Unpaired *t*-test: ***p < 0.001. Paraffin sections; scale bars: **A, B, D**, bar = 25 μm; **C** = 15 μm.

SC and motor nuclei of the brain stem in humans and mice, which are identified as C-boutons on the basis of single immunohistochemistry, and double- and triple-labeling immunofluorescence and confocal microscopy. C-boutons are pre-synaptic terminals of cholinergic interneurons localized in the SC and in most of the motor nuclei of the cranial nerves excepting the oculomotor nuclei of the brainstem (41–47). They contain VAChT and synaptic vesicle markers, and are in contact with postsynaptic components including M2 muscarinic receptors and S1R; neuregulin 1-ErB retrograded signaling is also differentially compartmentalized in C-type boutons (43, 46–49). Cholinergic

interneurons modulate motor neuron activity through C-boutons (43–45, 50). On the basis of the present findings, LRRC50 may be considered a component of C-boutons involved in dynein assembly and retrograde axonal transport.

　　In agreement with our previous gene transcription observations, *DNAAF1* mRNA expression is reduced in the SC anterior horn in sALS cases. Reduced *DNAAF1* mRNA expression can be the result of mere motor neuron demise. However, LRRC50 immunoreactivity is drastically reduced at the surface of the remaining spinal and bulbar motor neurons, in parallel with reduced numbers of C-boutons, in sALS.

7
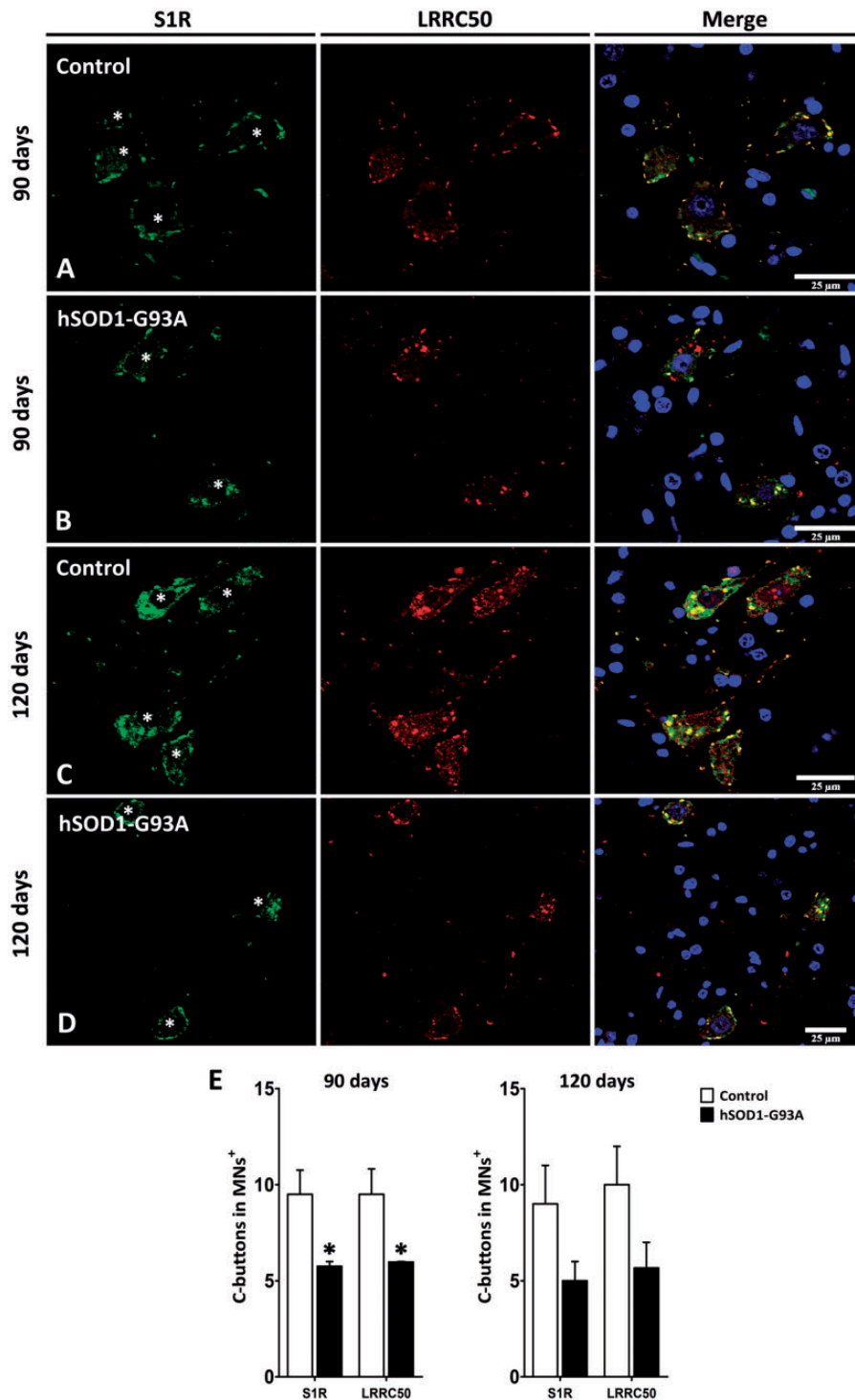
FIGURE 5. LRRC50 (red) and S1R (green) immunoreactivity in motor-neurons of the ventral horn of the spinal cord in control and *hSOD1-G93A* transgenic mice aged 90 **(A, B)** and 120 **(C, D)** days. LRRC50 and S1R immunoreactivity is decreased in transgenic animals when compared with controls **(A–D)**, although some LRRC50- and S1R-positive structures are still present in neurons in transgenic mice. Asterisks indicate the localization of the cytoplasm of motor neurons. **(E)** Quantitative studies show a significant decrease in the number of LRRC50- and S1R-immunoreactive structures in transgenic mice aged 90 days (preclinical stage) and a trend at the age of 120 days when compared with control littermates. Unpaired *t*-test: *$p < 0.05$. Paraffin sections; scale bar $= 25 \,\mu m$.

Therefore, LRRC50 reduction is not the mere reflection of motor neuron demise but a reduction in the number of LRRC50-immunoreactive boutons in the remaining motor neurons in sALS.

This decline occurs independently of the aberrant formation of TDP-43-immunoreactive inclusions in certain motor neurons in classical sALS (7, 8). This decline neither corelates with the appearance of dynein-dynactin-immunoreactive deposits in motor neurons, which are also not related with skein-like inclusions, in the SC in sALS (51). However, LRRC50 reduction in C-boutons is accompanied by perinuclear LRRC50 immunoreactivity in some remaining motor neurons thus suggesting some kind of alteration in the transport of this protein.

Loss of cholinergic synapses in the SC motor-neurons in sALS was reported many years ago (52). That pioneering observation was not studied further in humans but was partially refuted in SOD1 transgenic mice (53, 54). This is due in part to the different markers used to detect C-boutons in SOD1 transgenic mice. A significant increase in the number of NRG1-positive boutons was observed at the beginning of the symptomatic stage which was followed by a marked decrease at end stages of the disease. A similar pattern occurred for VAChT boutons, but some motor-neurons depleted of VAChT-immunoreactive boutons showed high numbers of NRG1-positive dots (46). Our present observations show a marked reduction in LRRC50-immunoreactive boutons in motor neurons of the ventral horn in *hSOD1-G93A* transgenic mice aged 150 days which is accompanied by a parallel decrease in, but not the absence of, S1R-immunoreactive boutons. The presence of the remaining S1R seems to be protective of motor neurons, as the knocking-out of S1R in *hSOD1-G93A* transgenic mice exacerbates motor neuron disease progression in these animals (55). Early pre-symptomatic alterations in C-boutons has been reported in SOD1(G93A) tg mice (56). Interestingly, viral-mediated delivery of type III-NRG1 to the SC restores the number of C-boutons and extends the survival time of SOD1-ALS mice (57).

Our combined study in human sALS not linked to SOD1 mutations and in transgenic mice bearing high copy numbers of the mutated form of human SOD1 show common responses regarding C-boutons in motor neurons. The number of LRRC50-immunoreactive structures is decreased in motor neurons in both paradigms. To learn whether observed alterations in ALS are early or late events, transgenic mice at preclinical, early clinical and late clinical stages were examined. A decrease in LRRC50 immunoreactivity occurs at preclinical stages in hSOD1-G93A transgenic mice, suggesting that LRRC50 alteration is an early event in the course of the disease. A trend to decrease is observed at the age of 120; lack of significance can be due to the relative low number of animals examined or to a transient attempt to compensation. However, a significant decrease is manifested at the age of 150 days.

The pattern of C-bouton response in sALS and Tg mice differs from that seen after nerve peripheral nerve axotomy in mice. Reduced expression of VAChT and NRG1 immunoreactivity together with a reduction in size of C-boutons starting at 24 hours is followed by practical recovery by 30 days postlesion (47, 58). Therefore, the changes observed here in motor neuron disease are hardly due to peripheral axotomy.

Whether LRRC50 in motor neurons is essential for the maintenance of C-boutons cannot be addressed by neuropathological approach. Yet this is an important point for understanding the role of this protein in motor neuron maintenance and neurodegeneration.

ACKNOWLEDGMENTS

REFERENCES

1. Maday S, Twelvetrees AE, Moughamian AJ, et al. Axonal transport: Cargo-specific mechanisms of motility and regulation. Neuron 2014;84: 292–309
2. Hirokawa N, Niwa S, Tanaka Y. Molecular motors in neurons: Transport mechanisms and roles in brain function, development and disease. Neuron 2010;68:610–38
3. Roberts AJ, Kon T, Knight PJ, et al. Functions and mechanics of dynein motor proteins. Nat Rev Mol Cell Biol 2013;14:713–26
4. Vallee RB, McKenney RJ, Ori-McKenney KM. Multiple modes of cytoplasmic dynein regulation. Nat Cell Biol 2012;14:224–30
5. Carter AP. Crystal clear insights into how the dynein motor moves. J. Cell Sci 2013;126:705–13
6. Jaarsma D, Hoogenraad CC. Cytoplasmic dynein and its regulatory proteins in Golgi pathology in nervous system disorders. Front Neurosci 2015;9:e397
7. Strong MJ, Hortobágyi T, Okamoto K, et al. Amyotrophic lateral sclerosis, primary lateral sclerosis, and spinal muscular atrophy. In: Dickson DW, Weller RO, eds. Neurodegeneration: The Molecular Pathology of Dementia and Movement Disorders. 2nd edn. Oxford: Wiley-Blackwell 2011:418–33
8. Ince PG, Highley JR, Wharton SB. Motor neuron disorders. In: Love S, Budka H, Ironside JW, Perry A, eds. Greenfield's Neuropathology. 9th edn. Boca Raton: CRC Press, Taylor and Francis Group 2015:817–48
9. LaMonte BH, Wallace KE, Holloway BA, et al. Disruption of dynein/dynactin inhibits axonal transport in motor neurons causing late-onset progressive degeneration. Neuron 2002;34:715–27
10. Hafezparast M, Klocke R, Ruhrberg C, et al. Mutations in dynein link motor neuron degeneration to defects in retrograde transport. Science 2003;300:808–12
11. Münch C, Sedlmeier R, Meyer T, et al. Point mutations of the p150 subunit of dynactin (DCTN1) gene in ALS. Neurology 2004;63:724–6
12. Bruijn LI, Miller TM, Cleveland DW. Unraveling the mechanisms involved in motor neuron degeneration in ALS. Annu Rev Neurosci 2004; 27:723–49
13. Ligon LA, LaMonte BH, Wallace KE, et al. Mutant superoxide dismutase disrupts cytoplasmic dynein in motor neurons. NeuroReport 2005;16: 533–6
14. Levy JR, Holzbaur E. Cytoplasmic dynein/dynactin function and dysfunction in motor neurons. Int J Dev Neurosci 2006;24:103–11
15. Teuling E, van Dis V, Wulf PS, et al. A novel mouse model with impaired dynein/dynactin function develops amyotrophic lateral sclerosis (ALS)-like features in motor neurons and improves lifespan in SOD1-ALS mice. Hum Mol Genet 2008;17:2849–62
16. Deng W, Garrett C, Dombert B, et al. Neurodegenerative mutation in cytoplasmic dynein alters its organization and dynein-dynactin and dynein-kinesin interactions. J Biol Chem 2010;285:39922–34
17. Kuźma-Kozakiewicz M, Chudy A, Kaźmierczak B, et al. Dynactin deficiency in the CNS of humans with sporadic ALS and mice with genetically determined motor neuron degeneration. Neurochem Res 2013;38: 2463–73
18. Ikenaka K, Kawai K, Katsuno M, et al. Dnc-1/dynactin 1 knockdown disrupts transport of autophagosomes and induces motor neuron degeneration. PLoS One 2013;8:e54511

19. Andrés-Benito P, Moreno J, Aso E, et al. Amyotrophic lateral sclerosis, gene deregulation in the anterior horn of the spinal cord and frontal cortex area 8: Implications in frontotemporal lobar degeneration. Aging 2017;9:823–51

20. Van Rooijen E, Giles RH, Voest EE, et al. LRRC50, a conserved ciliary protein implicated in polycystic kidney disease. J Am Soc Nephrol 2008; 19:1128–38

21. Loges NT, Olbrich H, Becker-Heck A, et al. Deletions and point mutations of LRRC50 cause primary ciliary dyskinesia due to dynein arm defects. Am J Hum Genet 2009;85:883–9

22. Hartill VL, van de Hoek G, Patel MP, et al. DNAAF1 links heart laterality with the AAA+ ATPase RUVBL1 and ciliary intraflagellar transport. Hum Mol Genet 2018;27:529–45

23. Andrés-Benito P, Domínguez R, Colomina MJ, et al. YKL40 in sporadic amyotrophic lateral sclerosis: Cerebrospinal fluid levels as a prognosis marker of disease progression. Aging (Albany NY) 2018;10:2367–82

24. Vancoillie G, Lambert J, Mulder A, et al. Cytoplasmic dynein colocalizes with melanosomes in normal human melanocytes. Br J Dermatol 2000; 143:298–306

25. Chuang JZ, Milner TA, Sung CH. Subunit heterogeneity of cytoplasmic dynein: Differential expression of 14 kDa dynein light chains in rat hippocampus. J Neurosci 2001;21:5501–12

26. Jha R, Surrey T. Regulation of processive motion and microtubule localization of cytoplasmic dynein. Biochem Soc Trans 2015;43:48–57

27. Twelvetrees AE, Pernigo S, Sanger A, et al. The dynamic localization of cytoplasmic dynein in neurons is driven by kinesin-1. Neuron 2016;90: 1000–15

28. Omran H, Kobayashi D, Olbrich H, et al. Ktu/PF13 is required for cytoplasmic pre-assembly of axonemal dyneins. Nature 2008;456:611–6

29. Kott E, Duquesnoy P, Copin B, et al. Loss of zinc finger MYND-type containing 10 (zmynd10) affects cilia integrity and axonemal localization of dynein arms, resulting in ciliary dysmotility, polycystic kidney and scoliosis in medaka (*Oryzias latipes*). Dev Biol 2017;430:69–79

30. Tarkar A, Loges NT, Slagle CE, et al. DYX1C1 is required for axonemal dynein assembly and ciliary motility. Nat Genet 2013;45:995–1003

31. Inaba Y, Shinohara K, Botilde Y, et al. Transport of the outer dynein arm complex to cilia requires a cytoplasmic protein Lrrc6. Genes Cells 2016; 21:728–39

32. Jaffe KM, Grimes DT, Schottenfeld-Roames J, et al. c21orf59/kurly controls both cilia motility and polarization. Cell Rep 2016;14:1841–9

33. Mali GR, Yeyati PL, Mizuno S, et al. ZMYND10 functions in a chaperone relay during axonemal dynein assembly. eLife 2018;7:e34389

34. Moore DJ, Onoufriadis A, Shoemark A, et al. Mutations in ZMYND10, a gene essential for proper axonemal assembly of inner and outer dynein arms in humans and flies, cause primary ciliary dyskinesia. Am J Hum Genet 2013;93:346–56

35. Zariwala MA, Gee HY, Kurkowiak M, et al. ZMYND10 is mutated in primary ciliary dyskinesia and interacts with LRRC6. Am J Hum Genet 2013;93:336–45

36. Kurkowiak M, Ziętkiewicz E, Greber A, et al. ZMYND10-mutation analysis in Slavic patients with primary ciliary dyskinesia. PLoS One 2016; 11:e0148067

37. Cho KJ, Noh SH, Han SM, et al. ZMYND10 stabilizes intermediate chain proteins in the cytoplasmic pre-assembly of dynein arms. PLoS Genet 2018;14:e1007316

38. Höbean IM, Hjeij R, Olbrich H, et al. Mutations in C11orf70 cause primary ciliary dyskinesia with randomization of left/right body asymmetry due to defects of outer and inner dynein arms. Am J Hum Genet 2018; 102:973–84

39. Fassad MR, Shoemark A, le Borgne P, et al. C11orf70 mutations disrupting the intraflagellar transport-dependent assembly of multiple axonemal dyneins cause primary ciliary dyskinesia. Am J Hum Genet 2018;102: 956–72

40. Olcese C, Patel MP, Shoemark A, et al. X-linked primary ciliary dyskinesia due to mutations in the cytoplasmic axonemal dynein assembly factor PIH1D3. Nat Commun 2017;8:14279

41. Conradi S. Ultrastructure and distribution of neuronal and glial elements on the surface of the proximal part of a motoneuron dendrite, as analyzed by serial sections. Acta Physiol Scand Suppl 1969;332:49–64

42. Hellstrom J, Arvidsson U, Elde R, et al. Differential expression of nerve terminal protein isoforms in VAChT-containing varicosities of the spinal cord ventral horn. J Comp Neurol 1999;411:578–90

43. Miles GB, Hartley R, Todd AJ, et al. Spinal cholinergic interneurons regulate the excitability of motoneurons during locomotion. Proc Natl Acad Sci U S A 2007;104:2448–53

44. Zagoraiou L, Akay T, Martin JF, et al. A cluster of cholinergic premotor interneurons modulates mouse locomotor activity. Neuron 2009;64: 645–62

45. Frank E. A new class of spinal interneurons: The origin and function of C-bouton solved. Neuron 2009;64:593–5

46. Gallart-Palau X, Tarabal O, Casanovas A, et al. Neuregulin-1 is concentrated in the postsynaptic subsurface cistern of C-bouton inputs to motoneurons and altered during motoneuron diseases. FASEB J 2014;28: 3618–32

47. Casanovas A, Salvany S, Lahoz V, et al. Neuregulin 1-ErbB module in C-bouton synapses on somatic motor neurons: Molecular compartmentation and response to peripheral nerve injury. Sci Rep 2017;7:40155

48. Hellstrom J, Oliveira ALR, Meister B, et al. Large cholinergic nerve terminals on subsets of motoneurons and their relation to muscarinic receptor type 2. J Comp Neurol 2003;460:476–86

49. Mavlyutov TA, Epstein ML, Andersen KA, et al. The sigma-1 receptor is enriched in postsynaptic sites of C-terminals in mouse motoneurons. An anatomical and behavioral study. Neuroscience 2010;167:247–55

50. Witts EC, Zagoraiou L, Miles GB. Anatomy and function of cholinergic C bouton inputs to motor neurons. J Anat 2014;224:52–60

51. Ateh DD, Hussain IK, Mustafa AH, et al. Dynein-dynactin complex subunits are differentially localized in brain and spinal cord, with selective involvement in pathological features of neurodegenerative disease. Neuropathol Appl Neurobiol 2007;34:88–94

52. Nagao M, Misawa H, Kato S, et al. Loss of cholinergic synapses on the spinal motor neurons of amyotrophic lateral sclerosis. J Neuropathol Exp Neurol 1998;57:329–33

53. Pullen AH, Athanasiou D. Increase in presynaptic territory of C-terminals on lumbar motoneurons of G93A SOD1 mice during disease progression. Eur J Neurosci 2009;29:551–61

54. Herron LR, Miles GB. Gender-specific perturbations in modulatory inputs to motoneurons in a mouse model of amyotrophic lateral sclerosis. Neuroscience 2012;226:313–23

55. Mavlyutov TA, Epstein ML, Verbny YI, et al. Lack of sigma-1 receptor exacerbates ALS progression in mice. Neuroscience 2013;240:129–34

56. Casas C, Herrando-Grabulosa M, Manzano R, et al. Early presymptomatic cholinergic dysfunction in a murine model of amyotrophic lateral sclerosis. Brain Behav 2013;3:145–58

57. Lasiene J, Komine O, Fujimori-Tonou N, et al. Neuregulin 1 confers neuroprotection in SOD1-linked amyotrophic lateral sclerosis mice via restoration of C-boutons of spinal motor neurons. Acta Neuropathol Commun 2016;4:15

58. Sumner BE. A quantitative analysis of boutons with different types of synapse in normal and injured hypoglossal nuclei. Exp Neurol 1975;49: 406–17